

High-Temperature Wireless Sensor Platform Powered by Energy Scavenging

SHANE WINTERS¹ (Student Member, IEEE), NIKUNG THAPA¹, LUKE D. DOUCETTE¹, JONATHAN KINCAID¹ (Member, IEEE), QINGSONG CUI², NURI W. EMANETOGLU¹ (Member, IEEE), AND MAURICIO PEREIRA DA CUNHA¹ (Senior Member, IEEE)

¹Frontier Institute for Research in Sensor Technologies, University of Maine, Orono, ME 04469 USA

²Department of Physics, Astronomy, Geoscience, and Engineering Technology, Valdosta State University, Valdosta, GA 31698 USA

CORRESPONDING AUTHOR: MAURICIO PEREIRA DA CUNHA (e-mail: mdacunha@maine.edu)

This work was supported in part by the U.S. Department of Energy, Office of Science, Office of Basic Energy Sciences Established Program to Stimulate Competitive Research under Grant DE-SC0021981; and in part by the NSF Program "REU Site: Sensor Science and Engineering" under Grant 1851998.

ABSTRACT This article reports on the development of key components required for a self-powered oscillator unit designed to wirelessly transmit its signal under full insertion in high-temperature (HT) harsh-environments (HE), such as those present in power plants and industrial settings (metallurgic, oil extraction, molding, and aerospace). The oscillator employed a silicon carbide power transistor and HT passive components on a screen-printed alumina circuit board capable of operation beyond 300 °C. The HT oscillator circuit was powered solely by in-situ energy-scavenging thermoelectric generator (TEG) modules using passive cooling, eliminating the need for an external power supply or active cooling. In addition, a silicon-based external booster circuit was used to achieve the required TEG voltage regulation to test the TEG-powered HT oscillator circuit. The TEG-powered oscillator circuit was tested inside a nonmetallic furnace from room temperature to over 300 °C for transmission of a wireless signal, which was detected outside the furnace at 11 ft (3.4 m). Such a wireless transmitting system powered only by in-situ TEGs, with no requirement for external power or active cooling, is very attractive for flexible, mobile standalone control and sensor units targeted for operation in HT HE conditions found in power plants and industrial settings.

INDEX TERMS Energy scavenging, harsh-environment (HE), high-temperature (HT), high-temperature (HT) oscillator, industrial application, silicon carbide (SiC), thermoelectric generator (TEG), wireless.

I. INTRODUCTION

THE need for self-powered wireless sensor systems and associated electronic circuitry that can function in high-temperature (HT) harsh-environment (HE) conditions is a persistent theme in the power generation [1], downhole drilling [2], [3], [4], aerospace [5], and process control [6] industries. In the absence of such HT HE sensor data, mathematical modeling, predictive programming, and statistical techniques are used to predict faults and optimize the scheduling of inspections and maintenance downtimes [1], [4]. In spite of the importance of the aforementioned techniques, there is still a strong demand for in-situ sensors and systems that can respond to the following needs: 1) provide real-time data information to allow in-situ monitoring of equipment and plants, and checking their deterioration that could

otherwise lead to larger and more costly failures; 2) avoid costly operational downtimes required to perform service inspections; 3) perform planned maintenance to avoid catastrophic system failure; and 4) ensure safe operation in hostile environments [4]. Wireless surface acoustic wave resonator (SAWR) sensor systems have been shown to be a promising technology for HT HE monitoring applications [7]. SAWR devices can operate as passive batteryless sensors, but the lack of active circuits capable of providing signal processing and amplification at HT limits the interrogation distance.

Silicon carbide (SiC), having a large bandgap of 3.3 eV, is an attractive semiconductor for the design and implementation of HT oscillator-based wireless sensor systems. Continuous stable operation of SiC junction field effect transistors at temperatures above 500 °C for as long as 1 year has been

demonstrated [8] and SiC devices have maintained semiconductor functionality at temperatures as high as 961 °C [9]. However, the use of active electronic components, such as transistors, demands a power source for operation. Several energy-scavenging techniques have been considered for use with sensors, which include energy sources, such as vibration, air flow, solar, phase change materials, bioenergy, hydrogen reactions, water energy, geothermal energy, and different energy extraction methods, such as piezoelectric, electrostatic, and electromagnetic [10], [11]. Despite the attempt to use SiC technology for harsh-temperature applications [12], [13], [14], [15], [16], none of the previously mentioned energy-scavenging alternatives have been employed to power commercially available SiC transistor circuits at milliwatts or higher power consumption values inside an HT HE for fully standalone and wireless operation.

Thermal energy scavenging presents itself as an appropriate alternative for powering HT SiC-based electronics due to the availability of thermoelectric generators (TEGs) capable of delivering the power required for biasing the SiC transistors and potential operation up to 900 °C [17]. TEG power modules are based on the Seebeck effect, utilizing this principle to generate a differential voltage between cold and hot regions of both P and N doped materials that make up each module. As such, this energy harvesting technology is very attractive to power circuits in applications subject to appropriate temperature gradients. TEG technology has been used in diverse HE applications, including interplanetary probes [18], deep-sea hydrothermal energy scavenging [19], and combustion engine waste heat recovery systems [20]. Other targets for TEG energy scavenging have included ocean-going ships, locomotives, woodstove heat, human body heat, solar panel waste heat [21], and an ultrasound system for dry cask nuclear fuel storage monitoring [22]. Recent work has successfully demonstrated the use of a TEG to exploit the temperature gradient of the inside/outside of a window frame during wintertime to power a silicon-based wireless sensor network in a room-temperature environment [23]. Others have performed modeling investigations on the potential usage of TEGs to power wireless systems to monitor spent nuclear fuel in dry-cask storage [24], and more recently, TEG technology was considered for harvesting waste heat in a nuclear power plant to power a silicon-based wireless sensor system located outside of the HE [25].

This article reports on an HT SiC-based oscillator circuit powered by a TEG energy-scavenging power source through an Si-based booster circuit to condition the TEG output voltage. The oscillator circuit signal was wirelessly transmitted from within the HT environment (>300 °C) and detected by an antenna positioned 11 ft (3.4 m) away from the furnace with a signal intensity of -47 dBm. The successful implementation of this system represents the initial steps toward developing a more compact and standalone sensor system, capable of wirelessly transmitting a sensor signal from within an HT hostile environment.

The HT oscillator circuit was fabricated using a commercially available SiC metal oxide semiconductor field effect transistor (MOSFET) and HT commercial and in-house fabricated passive components integrated on a screen-printed alumina circuit board capable of operation beyond 300 °C. The HT electronics were then integrated with passively cooled TEG modules, which were used to power the circuitry with a hot and cold sides temperature difference (ΔT) in between 20 °C and 40 °C. No other external power source was used to either bias or cool the entire integrated system. To boost up the biasing voltage applied to the oscillator circuit, a room-temperature power-conditioning module (booster circuit) was employed. The booster circuit also served to improve the voltage regulation of the TEGs. This booster circuit was connected to the output of TEGs and kept outside of the test furnace that enabled the HT testing of the TEG-powered SiC-based oscillator circuit. Other than this booster circuit unit, the integrated SiC oscillator-TEG powered system was assembled in an HT nonmetallic furnace to allow for wireless transmission and system testing at temperatures beyond 300 °C.

The energy scavenging and oscillator circuit implemented and integrated in this article demonstrate the capability of key components to operate as a self-powered wireless sensor and monitoring system in power plants and HT HE industrial applications.

The rest of this article is organized as follows. Section II discusses the principles of operation of both HT SiC oscillator circuit and TEG implemented. Section III addresses details of the oscillator circuit, the energy-scavenging system, the nonmetallic furnace, the wireless link, and the integration of all these components. Section IV presents the measured performance of Section III components and the overall integrated system. Finally, Section V concludes this article.

II. OSCILLATOR CIRCUIT AND TEG DESIGN, SIMULATION, AND OPERATION

A. OSCILLATOR CIRCUIT DESIGN

To meet the requirements of HT operation and wireless signal transmission, the source-follower-based Colpitts oscillator circuit shown in Fig. 1 was used in this article. Fig. 1 shows the circuit components, which include resistors, capacitors, an inductor, and their respective values. The Colpitts oscillator uses an inductor-capacitor (LC) tank circuit with a capacitive divider [26].

Simplicity and a low component count were targeted to diminish the probability of circuit failure due to component degradation when exposed to long-term operation at HTs (>300 °C for the purposes of this article). In this design, the output of the source-follower is fed back to its input via an LC tank circuit and an 82 nF alternating current (ac) coupling capacitor C_3 . From the well-known Barkhausen criterion [27], this circuit will oscillate at the resonant frequency of the LC

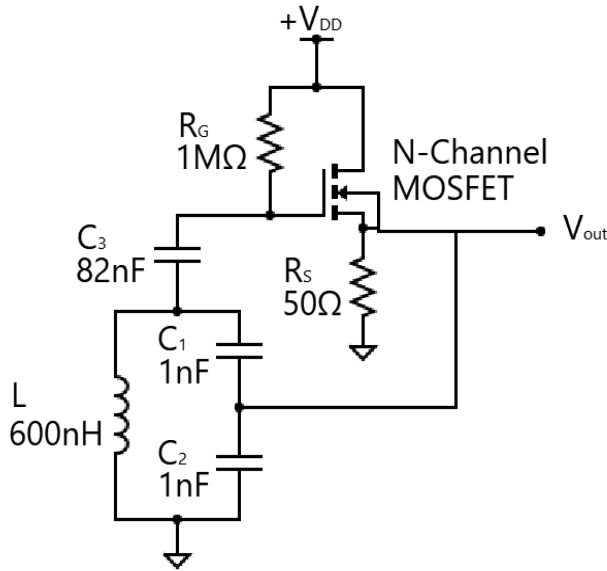


FIGURE 1. Simplified source-follower Colpitts oscillator circuit used in this article.

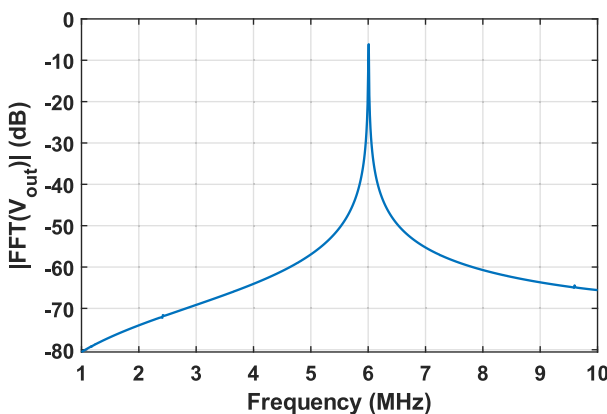


FIGURE 2. Simulated FFT of V_{out} from the oscillator circuit shown in Fig. 1.

tank circuit, given by

$$f_{osc} = \frac{1}{2\pi\sqrt{LC_T}}, \text{ where } C_T = \frac{C_1 C_2}{C_1 + C_2}. \quad (1)$$

This equation gives $f_{osc} \cong 9.2$ MHz at room temperature for the nominal component values shown in Fig. 1, if the parasitic capacitances of the transistor are ignored. The bare die CPM3-1200-0075A N-Channel SiC power MOSFET (Cree/Wolfspeed, North Carolina) used in this article has a nominal input capacitance of $C_{iss} = 1.56$ nF, comparable to the capacitors in the tank circuit, which shifts the oscillation frequency downward. The circuit was simulated with LTSpice and Microcap simulation tools, using the model provided by Cree/Wolfspeed. These simulations predicted an oscillation frequency of $f_{osc} \cong 6.0$ MHz at room temperature. A fast-Fourier transform of the simulated source-follower oscillator circuit output voltage, V_{out} , is shown in Fig. 2.

The source-follower circuit's gain and phase characteristics are critical to the oscillator functioning. These are dependent on the bias current I_D of the transistor, which in turn is determined by the transistor's transconductance k_n and threshold voltage V_{tn} , as well as the source resistor R_S . Neglecting secondary effects, the drain current in saturation is given by [28]

$$I_D = \frac{1}{2}k_n((V_G - V_S) - V_{tn})^2 \quad (2)$$

where the MOSFET source voltage is $V_S = I_D R_S$. According to the CPM3-1200-0075A datasheet [29], V_{tn} can vary between 1.8 and 3.6 V from device to device at room temperature, with a typical value of 2.5 V. Additionally, the threshold voltage will decrease as the ambient temperature increases from room temperature, as further identified in this article in Section IV-A. While the SiC transistors used in these experiments are power MOSFETs, the bias levels of the circuit do not reach the values where the MOSFET behavior would deviate from the standard MOSFET I-V relation in saturation given in (2). The gate voltages were 6 V or less and the peak current draw was less than 200 mA, significantly below the ratings of the device. The source resistor R_S provides negative feedback to keep I_D in the design range. As V_{tn} decreases with increasing temperature, I_D will increase. However, this increase in I_D will increase V_S , which in turn reduces I_D , thus working toward the stabilization of V_{out} over a wide range of temperature.

A voltage divider would normally be used to set the gate bias voltage for the source-follower circuit shown in Fig. 1. However, this circuit has only the gate resistor R_G between the supply voltage V_{DD} and the gate, setting the gate voltage $V_G = V_{DD}$. This was done to ensure that the circuit would turn ON as soon as the TEG supply and associated booster circuit generated sufficient voltage and power from the HE.

The inductor L in the LC tank circuit was used as the wireless radiating element, since the radiating signal from L was large enough to be easily detected several meters away from the HT circuit.

B. THERMOELECTRIC GENERATOR OPERATION

The Seebeck effect is a thermoelectric phenomenon in which a temperature difference between two ends of a conductive material induces a voltage between the respective extremities. The magnitude of the voltage difference depends on the magnitude of the temperature difference and the specific thermoelectric material. This relationship can be written as [30]

$$\Delta V = -S\Delta T \quad (3)$$

where ΔV (V) is the steady-state open-circuit voltage difference between the two ends of the thermoelectric material, ΔT (K) is the temperature difference between the TEG hot and cold sides, and S is the material dependent Seebeck coefficient (V/K). In general, if the TEG hot-side temperature is under a fixed value defined by the operating environment,

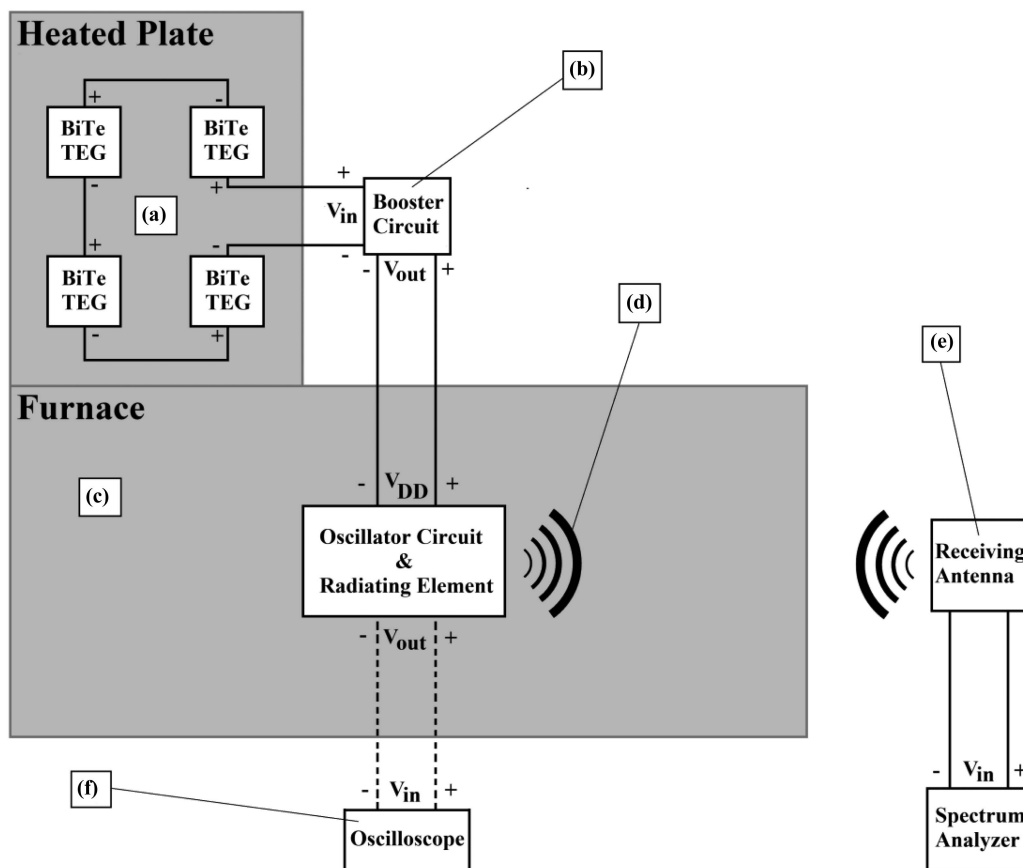


FIGURE 3. Overall block diagram of the experimental setup used in this article and further discussed in this section. (a) Four BiTe TEGs are connected in series and heated on a heated plate. (b) Room-temperature booster circuit is used to regulate and boost the voltage supplied by the TEGs. (c) In-house fabricated furnace is used to bring the oscillator circuit to the desired high temperature. (d) Wireless signal is transmitted by the oscillator from within the furnace. (e) Wireless signal is detected by an outside antenna connected to a spectrum analyzer. (f) Oscilloscope was also employed to optionally monitor the performance of the oscillator circuit.

the cold-side temperature must be kept as low as possible to optimize the ΔT value for generating a maximum ΔV . For this reason, TEGs are often used in conjunction with active-cooling methods, such as liquid circulation or fans to help reduce the cold-side temperature. However, such approaches require an external power source to drive the active-cooling mechanisms. To achieve the goal of a fully self-contained energy-scavenging system based on TEGs, active-cooling methods were specifically avoided in this article. Instead, passive cooling was employed using a heatsink mounted on the cold side of the TEGs exposed to ambient room-temperature conditions.

III. METHODS AND PROCEDURES

A. OVERALL BLOCK DIAGRAM

A high-level block diagram of the overall experimental setup is shown in Fig. 3 and will be detailed in the following subsections. Four series-connected TEGs were used to convert the thermal energy generated by a heated plate to electrical power. The heated plate, integrated with an in-house constructed furnace, was used to simulate hot-cold gradients, such as those encountered inside power plant boiler chambers. The output

of the TEGs is connected to the operating booster circuit outside the furnace, as discussed in the previous section, which in turn is connected to the oscillator circuit. The oscillator circuit in the furnace utilizes the circuit inductor as the radiating element (as described in Section II-A) to wirelessly transmit its signal to a receiving antenna connected to a spectrum analyzer outside the furnace. An optional oscilloscope external to the furnace was used to characterize and monitor the performance of the tested oscillator circuit.

B. TEG, HEATSINK, AND BOOSTER CIRCUIT SETUP

This subsection discusses the implementation of the TEG energy-scavenging system used to electrically power the oscillator circuit. Bismuth-telluride (BiTe, Bi_2Te_3) TEGs (Thermoelectric Conversion Systems Ltd.) were used in this article and selected for the following reasons: 1) commercial availability; 2) compact size, $40 \text{ mm} \times 40 \text{ mm} \times 4 \text{ mm}$ ($W \times L \times H$); 3) relatively low output resistance per device (between 2 and 3Ω); and 4) capability of delivering 1 to 1.5 V per device using only passive cooling (no forced cooling) at relatively reduced ΔT values ($20^\circ\text{C} < \Delta T < 40^\circ\text{C}$).

An aluminum heatsink with radiative fins (Wakefield-Vette) was attached to the TEG modules to improve the

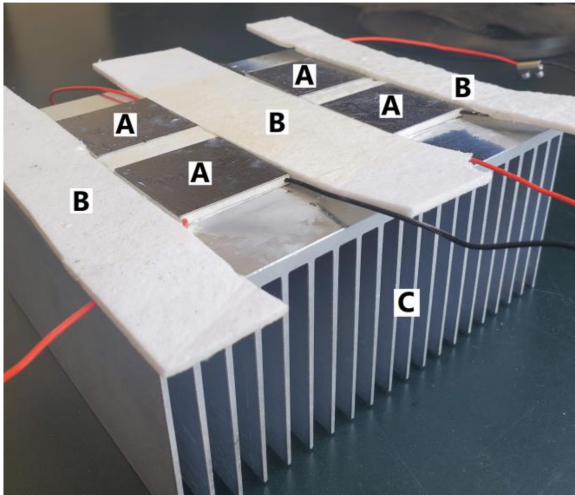


FIGURE 4. Hot-side view of four TEGs mounted onto a heatsink using thermal paste. (A) TEG devices. (B) Layers of insulation placed between the TEGs. (C) Heatsink fins.

passive cooling of the TEGs cold side (Fig. 4). The heatsink measured 7.38" L × 6.00" W × 3.11" H (187 mm L × 152 mm W × 79 mm H), which provided sufficient area to mount the four TEGs connected in series mentioned in Section III-A onto a single heatsink. The TEGs were mounted to the heatsink using thermal paste (MG Chemicals) to establish consistent heat transfer from the TEG cold sides to the heatsink. The thin strips of insulation, which can be seen in Fig. 4, were placed between the TEGs to ensure that a maximum thermal gradient was achieved across the TEG modules.

As shown in Fig. 3 and discussed in Section I and Section III-A, the external booster circuit (X0122 dc/dc converter, TXL Group, Inc.) was used as a buffer in-between the TEGs and the oscillator circuit. This device has a nominal output voltage of 6 V dc, with an input voltage range of 0.4–5.1 V. In addition to providing the desired biasing voltage, the booster circuit is assisted in regulating the TEG output voltage. Without the booster, the BiTe TEG modules tested did not produce the required voltage to drive the oscillator at its peak oscillation current, resulting in ceased oscillation. In particular, the periodic current demands by the oscillator circuit would cause a ripple voltage on the order of 2 V at the output of the TEGs. As a result, when the designed TEG array is connected directly to the oscillator, it would not provide a constant supply voltage at the required levels (3.3 V and above), and thus no oscillation would take place. Similar behavior was reported in [32] when powering low-temperature sensors with a TEG power module. To overcome this issue, they utilized a high valued electrolytic-based buffer capacitor (e.g., 12 mF) to minimize voltage drops due to the varying power demands of the sensor device employed.

As previously mentioned, the external booster circuit used to increase the voltage provided by the TEG also served to regulate the voltage. Since the goal of this article was to demonstrate certain key components of a standalone, wireless, HT sensor platform (i.e., the integration of TEG

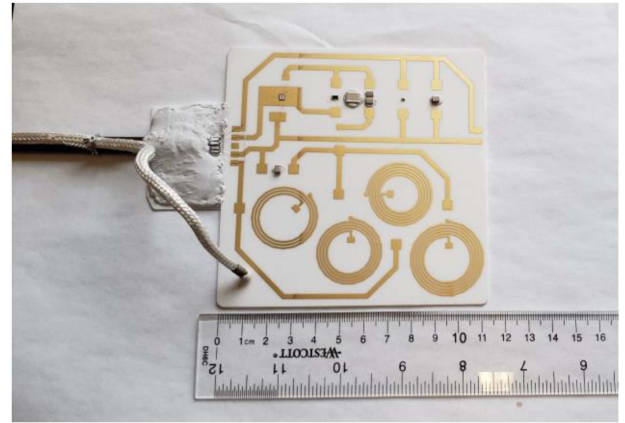


FIGURE 5. Oscillator circuit constructed on alumina circuit board with gold traces.

energy scavenging to power an SiC-based HT oscillator circuit), the development of an HT booster circuit and/or large capacitor that can operate at HTs to regulate the voltage was reserved for future article.

C. OSCILLATOR CIRCUIT IMPLEMENTATION AND WIRED MEASUREMENTS

The oscillator circuit schematic discussed in Section II-A (Fig. 1) was fabricated using gold paste silk-screen printing technique [31] on an alumina board (Fig. 5) capable of operation at HTs. As discussed in Section II-A, the commercially available bare die SiC MOSFET (P/N CPM3-1200-0075A) was used to implement the oscillator circuit. Passive circuit elements include Presidio HT ceramic capacitors (1 nF P/N HT1209NHT102K1P5; 82 nF P/N HT1725NHT823K1P5), Vishay resistors (50 Ω P/N PATT0603E49R9BGT1; 1 MΩ P/N CHPHT0805K1004FGT), and four custom designed gold printed planar–spiral inductors having different inductance values, which allowed for flexibility in circuit design and testing. The custom planar–spiral inductors were designed and simulated using Advanced Design System software (Keysight, California). Discrete circuit components were attached to the alumina board using an HT ceramic adhesive (Cotronics 940 HT) and were wire bonded using parallel gap resistance bonding equipment and 1 mil gold wire.

To electronically interface the circuit board with the TEGs and the optional monitoring oscilloscope, a pair of HT 50 Ω Inconel 600 coaxial cables (Thermocoax) were attached to the alumina board using the same HT adhesive, as shown in Fig. 5. One of the cables provides the required connection to the TEGs for powering the circuit. The other cable provides an option for in-situ monitoring and characterization of the circuit output and overall performance by connecting V_{out} to an external oscilloscope (Rigol DS1054Z). Finally, a K-type thermocouple (OMEGA Engineering) was mounted to the corner of the board and routed with the Inconel cables (Fig. 5) to monitor the circuit board temperature during the HT testing.

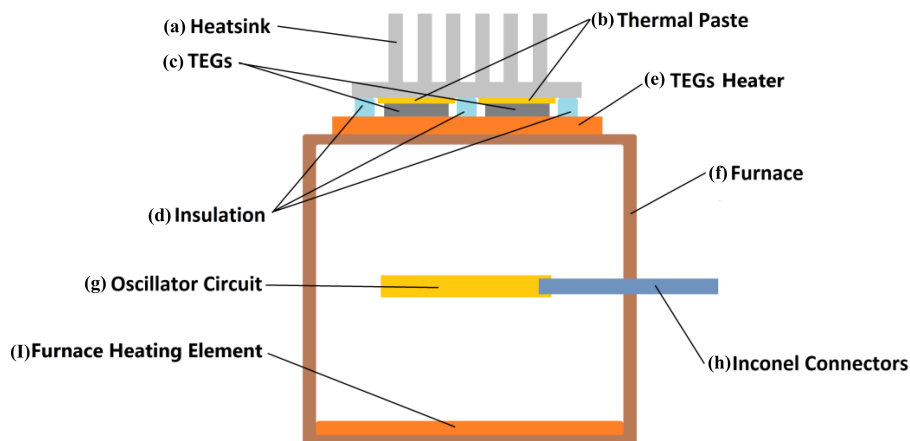


FIGURE 6. Sideview diagram of combined furnace, oscillator circuit, and TEGs Setup. (a) TEGs heatsink, (b) thermal paste, (c) TEGs, and (d) insulation associated with the TEGs setup shown in Fig. 4. (e) Heated plate to control the temperature of the TEGs. (f) Furnace box constructed from ceramic fiberboard insulation. (g) Oscillator circuit implemented on alumina board. (h) Two Inconel cables to: (i) connect the TEGs to the oscillator and (ii) to allow optional circuit monitoring via oscilloscope. (i) Furnace heating element.

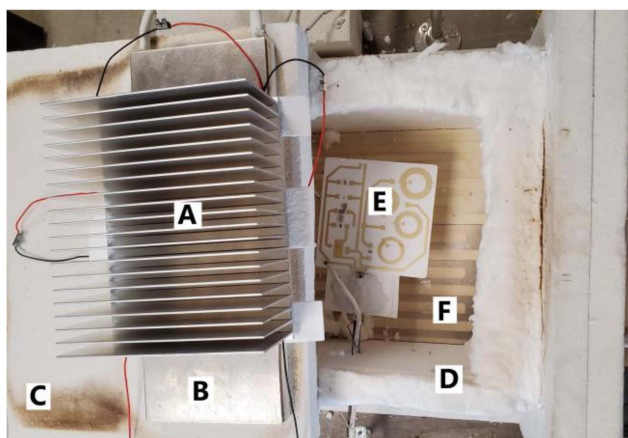


FIGURE 7. Top-down view of combined TEG/furnace/oscillator circuit setup, with top cover partially opened and shifted to the left so that the oscillator circuit is visible inside the furnace. (A) Heatsink and TEGs previously detailed in Fig. 4. (B) Heater for controlling TEG temperature. (C) Top cover of furnace. (D) Side wall of furnace, constructed from ceramic fiberboard. (E) Oscillator circuit, implemented on alumina board previously shown in Fig. 5. (F) Furnace heating element.

D. IN-HOUSE DESIGNED AND ASSEMBLED FURNACE

To test the wireless transmission from the SiC oscillator and TEG power integrated unit under HT operation, a nonmetallic furnace was designed and constructed using ceramic fiberboard insulation (Cotronics Corp). A diagram of the combined furnace with TEG/heatsink setup is shown in Fig. 6, and a top-down photograph of the setup is shown in Fig. 7. Also shown in Figs. 6 and 7 is a through-port in the furnace wall that allowed for 1) an Inconel cable to be routed from the TEG to the oscillator to power the circuit; 2) a second Inconel cable routed to the optional oscilloscope to monitor V_{out} ; and 3) a thermocouple probe (also shown in Fig. 5) to monitor the actual circuit temperature. The furnace employed a serpentine heating element (Watlow Electric Manufacturing Company) placed at the bottom and used a

proportional–integral–derivative controller to maintain the targeted temperature in the furnace within $\pm 2^\circ\text{C}$. The oscillator circuit was mounted inside this furnace, and the TEG/heatsink setup shown in Fig. 4 was mounted on top of the furnace to create a single, self-contained self-powered oscillator unit based solely on the temperature differences in the apparatus. The temperature to which the TEGs hot sides were exposed was controlled via the heated plate placed on top of the furnace, as discussed in Section III-A (Fig. 3) and represented in Fig. 6.

E. WIRELESS LINK

As depicted in Fig. 3, a receiving antenna in the room-temperature environment was used to detect the wireless signal transmitted by the oscillator circuit from inside the furnace. The inductor printed on the alumina board and located in the oscillator's feedback loop (Fig. 1) was found to radiate enough energy (as discussed in Sections II-A and III-A) to allow its use as an electrically small radiating antenna. The receiver antenna was implemented using a loop of copper wire, fastened to a wooden frame to provide mechanical support (diagram and photograph of the receiver antenna shown in Fig. 8). The receiver antenna placed outside the furnace was connected to an Agilent 9320A spectrum analyzer to measure the power spectrum of the received signal.

IV. RESULTS

A. EXTRACTION OF THE MOSFET I–V CURVES AS A FUNCTION OF TEMPERATURE

To characterize the operation of the Cree CPM3-1200-0075A SiC power MOSFET from room temperature to HTs (up to 350°C), a nonencapsulated transistor die was mounted and wire-bonded onto a test-jig using the same materials and methods described in Section III-C and tested in a Barnstead/Thermolyne F48015-60 box furnace. A Keithley 4200-SCS Semiconductor Characterization System was employed

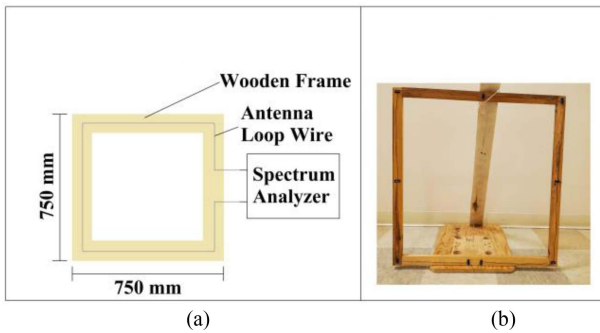


FIGURE 8. Wireless receiver setup. (a) Diagram of loop antenna connected to spectrum analyzer. (b) Photo of loop antenna.

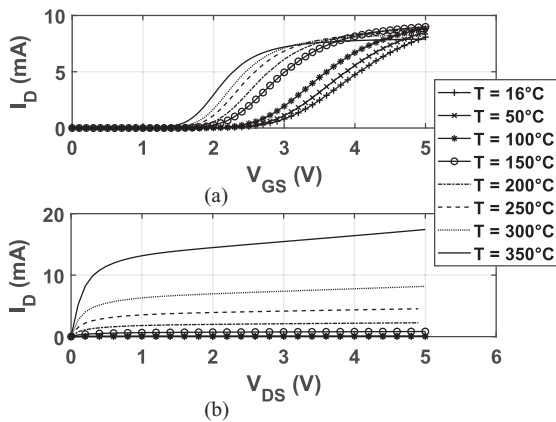


FIGURE 9. I-V curves at different temperature values for the Cree CPM3-1200-0075A SiC Power MOSFET. (a) Drain current vs. V_{GS} for $V_{DS} = 50$ mV. (b) Drain current vs. V_{DS} for $V_{GS} = 2.5$ V.

to obtain the SiC MOSFET I-V curves at eight specific temperature values (Fig. 9): 16 °C, 50 °C, 100 °C, 150 °C, 200 °C, 250 °C, 300 °C, and 350 °C. The transistor temperatures were measured with a K-type thermocouple mounted near the device. Fig. 9(a) plots the drain current I_D as a function of gate voltage V_{GS} at $V_{DS} = 50$ mV, whereas Fig. 9(b) plots I_D as a function of V_{DS} at $V_{GS} = 2.5$ V. These specific fixed values for V_{DS} and V_{GS} were selected because they provided I-V curves that were all within the current compliance range of the Keithley 4200-SCS for the range of temperatures that were tested.

The SiC MOSFET I_D - V_{GS} curves plotted in Fig. 9(a) were used to determine the threshold voltage V_{th} and show that V_{th} decreases as temperature increases. Therefore, the minimum voltage to initiate oscillation will decrease as temperature increases. The SiC MOSFET I_D - V_{DS} curves plotted in Fig. 9(b) reveal that I_D increases with temperature for a given value of V_{DS} voltage. This indicates that the output voltage of the oscillator should increase with temperature, though the negative feedback by the source resistor R_S will limit this increase.

B. HT OPERATION OF THE OSCILLATOR CIRCUIT

Three copies of the oscillator circuit described in Section III-C were constructed and tested for operation, using components with the same nominal values to check for consistency. Prior

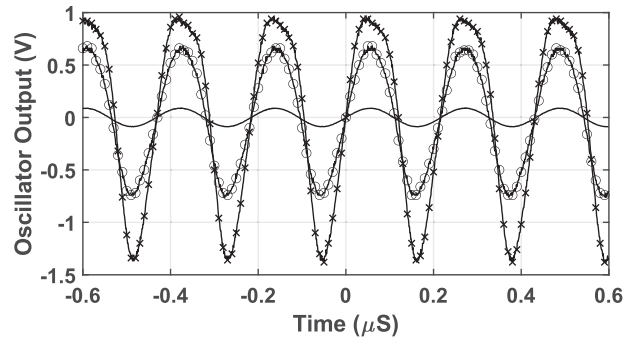


FIGURE 10. Typical oscillator circuit waveform (ac coupling mode) at 352 °C for three different values of power supply voltage. Curve (straight line): oscillator output at $V_{DD} = 3.3$ V. Curve (“o”): oscillator output at $V_{DD} = 4.5$ V. Curve (“x”): oscillator output at $V_{DD} = 6.0$ V. Note that $V_{DD} = 3.3$ V is the minimum bias voltage to operate the oscillator at this temperature.

to integration with the TEG power source, these circuits were tested up to 352 °C and over a range of bias voltages ($V_{DD} = 3.3, 4.5,$ and 6 V) using an external power supply (CSI3005XIII triple output 30 V dc power supply from circuit specialists) to characterize the circuit’s performance. These tests were done to confirm oscillator operation at HT and under varying bias conditions.

Fig. 10 is representative of the output voltage characteristics for an oscillator tested at 352 °C with three different power supply voltage settings: $V_{DD} = 3.3, 4.5,$ and 6 V. The lowest value is the minimum bias voltage required to sustain oscillation at 352 °C. The measurements were made with the ac coupling setting on the oscilloscope.

Consistent with the MOSFET characteristics shown in Fig. 9, the oscillator output increases with V_{DD} . Fig. 10 also shows that around $V_{DD} = 6$ V, the oscillator output starts to distort, indicating that the gate and source voltages are getting large enough for the MOSFET to enter the triode mode of operation.

C. CHARACTERIZATION OF TEG OUTPUT VOLTAGE VS. TEMPERATURE

Prior to integration with the SiC oscillator circuit, the voltage and current output of the TEGs were tested utilizing the experimental setup described in Section III-D (Figs. 6 and 7). As described in Section III-B (see Fig. 4), four TEGs were connected in series and the cold side mounted onto a heatsink for passive heat dissipation. No active cooling was employed in this article to fulfill the operational goal of a standalone unit, powered only by scavenged thermal energy.

The total open-circuit voltage of the TEGs connected in series was measured utilizing the TEGs heater shown in Figs. 6 and 7 as the sole heating dissipation aid. The total unloaded TEGs output voltage as a function of heated plate temperature is shown in Fig. 11(a) (blue discrete points). These measurements show that the TEG voltage increases with hot-side temperature in an approximately linear relationship as expected from (3). The four TEGs connected in series provide a total open-circuit voltage of 6.5 V when the heated plate temperature is set to 170 °C.

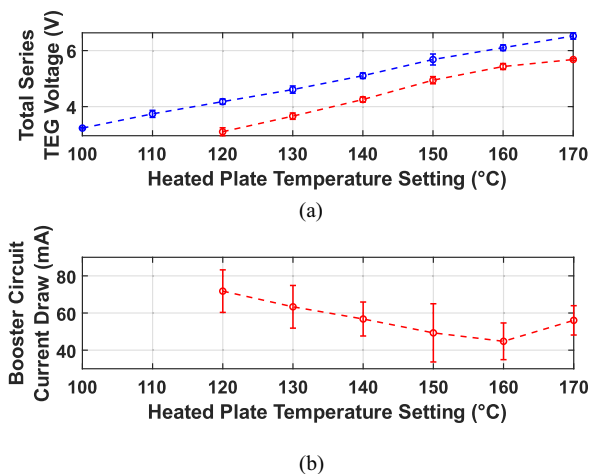


FIGURE 11. Voltage and current vs. heated plate temperature characteristics of four series-connected BiTe TEGs under passive heatsink cooling. (a) Total open-circuit TEGs voltage (blue curve); and the total TEGs voltage under loaded conditions, i.e., when connected to the booster/oscillator (red curve). (b) Current drawn from the TEGs by the booster/oscillator circuit, calculated using the measured total output resistance of $R_{out} = 14.9 \Omega$. Note: the dashed lines are included for clarity only as they connect the mean of each set of measured data points at each temperature. Data points in (a) and (b) represent the mean value of six measurements and the error bars represent ± 1 standard deviation.

After the characterization under unloaded condition, the TEGs were tested under different heated plate temperature settings while biasing the booster and oscillator circuits, which were kept at room temperature for this test. The red points in Fig. 11(a) show the results of the TEG system characterization under loaded conditions. If the heated plate temperature falls below 120°C , the voltage is not enough to operate the combination of booster and oscillator circuits. The voltage difference between open-circuit and loaded TEGs can be understood if the system is modeled as a Thevenin equivalent circuit with a source voltage equal to the total open-circuit voltage, and an output resistance R_{out} equal to the total output resistance of the TEGs plus the wires and connectors (measured to be approximately $R_{out} = 14.9 \Omega$).

Fig. 11(b) shows the current supplied to the booster circuit by the TEGs as a function of heated plate temperature setting. The current was calculated by using the voltage difference between open-circuit and loaded-circuit voltages divided by the output resistance R_{out} of the TEG system. The power drawn by the booster and oscillator circuit combination is relatively constant in this experiment, as they were maintained at room temperature for this test. The booster circuit current draw decreases as the heated plate temperature increases from 120°C to 160°C , which is explained by the increase of the supplied TEG voltage with temperature, and the constant load power. Between 160°C and 170°C , the current draw increases, as the voltage provided by the TEGs exceeded the booster circuit's reverse-biased input protection Zener diode's breakdown voltage, causing the diode to conduct current.

The results from Fig. 11 demonstrate that the passively cooled TEG/heatsink system can power the unheated

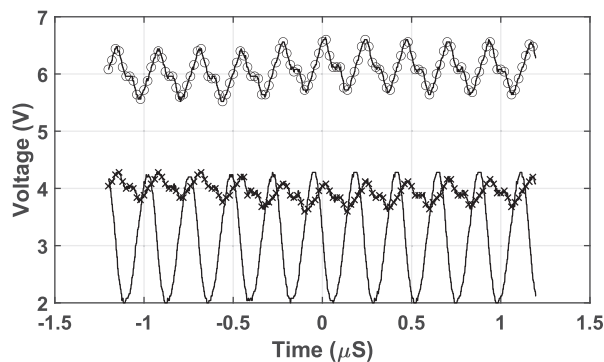


FIGURE 12. System tested under the following conditions: TEGs heated to 170°C and oscillator running around room temperature. Curve ("x"): TEG output voltage. Curve ("o"): booster circuit output voltage. Curve (straight line): oscillator circuit voltage output.

booster/oscillator system, when the TEGs were heated to at least 120°C on the hot side. Although 120°C is sufficient for powering the oscillator around room temperature, the experiments showed that the TEG system operated up to 170°C on the hot side provides the power required by the oscillator operating above 300°C .

D. OPERATION OF THE INTEGRATED TEG, BOOSTER, AND OSCILLATOR CIRCUITS FROM RT TO ABOVE 300°C

The fully integrated TEGs/booster/oscillator circuit system schematically depicted in Fig. 3 was characterized as a function of oscillator temperature using the test setup implemented and shown in Figs. 6 and 7.

Fig. 12 plots the voltage swings at the output of the TEGs system (TEGs curve, $\approx 0.5 V_{PP}$ ripple), at the output of the booster circuit (booster curve, $\approx 1 V_{PP}$ ripple), and at the output of the oscillator (oscillator curve, $\approx 2.2 V_{PP}$) when the TEGs system is subject to the heated plate at 170°C and the oscillator circuit operated unheated at room temperature.

As can be noted from Fig. 12, the ripple frequency matches the frequency of the oscillation, indicating that the voltage ripples are due to the periodic current demands of the oscillator. The selected booster circuit should operate with a 50 to 100 mV ripple under low output current conditions, at a frequency of 200 kHz defined by the internal clock oscillator of the booster circuit. However, under the conditions established by the oscillator circuit in this test, the booster circuit is unable to maintain the nominal ripple value mentioned above. The voltage ripple at the output of the TEGs is justified by the voltage drop across the TEGs output resistance R_{out} using the Thevenin equivalent circuit discussed in the previous section.

A supply bypass capacitor would normally be connected between the power and ground rails on the oscillator circuit to avoid this supply voltage ripple problem. It was determined both by calculation and experimentally (at room temperature) that a minimum bypass capacitor value around $1 \mu\text{F}$ would be appropriate for this circuit. However, the largest available HT capacitor value was 82 nF. Reaching the required supply bypass capacitor value by connecting these capacitors

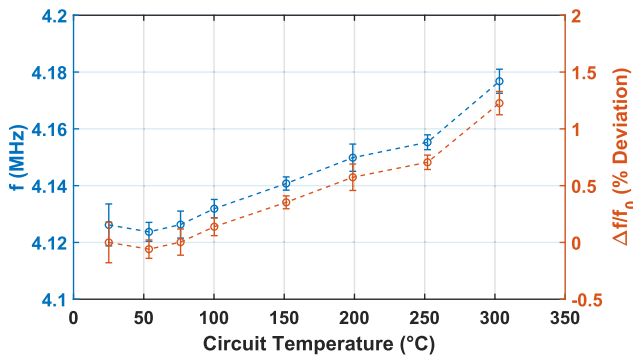


FIGURE 13. Oscillator circuit frequency vs. temperature for oscillator circuit powered by TEGs and booster circuit. Left axis (blue curve) shows the measured oscillation frequency in MHz for different circuit temperatures. Right axis (red curve) shows the measured oscillation frequency as a % deviation from the room temperature oscillation frequency. Data points for the oscillation frequency and oscillation frequency % deviation represent the mean value of 12 measurements and the error bars represent ± 1 standard deviation.

in parallel would have been prohibitively cumbersome and expensive, thus justifying the booster solution implemented in this article.

To simulate conditions commonly found within HT HE industrial and power plant settings, the oscillator circuit was tested from room temperature up to 300 °C, while the TEGs heated plate was maintained at 170 °C. The monitoring oscilloscope was used to measure the oscillating frequency (f), peak-to-peak output oscillator voltage (V_{PP}), and dc offset of the oscillator output (V_{RS}) as a function of temperature at eight discrete temperature values ranging from room temperature up to 300 °C, with 12 measurements averaged at each temperature.

Fig. 13 plots the oscillator frequency response (left axis) and the percent frequency variation (right axis) expressed as

$$\frac{\Delta f}{f_0} = 100 \frac{(f - f_0)}{f_0} \quad (4)$$

where f_0 is the frequency of oscillation at room temperature. A frequency variation of about 60 kHz was observed from room temperature to 300 °C, which corresponds to a $\Delta f/f_0$ value of 1.3%.

Fig. 13 also shows that the measured mean room-temperature oscillation frequency was around 4.125 MHz. This value is significantly lower than the 6 MHz simulation result presented in Section II-A for the room-temperature oscillation frequency. To explain this discrepancy, it is worth noting that a 47-cm long Inconel cable (50 Ω characteristic impedance) capable of operation above 900 °C connects the booster circuit to the oscillator. Analysis of this circuit implementation revealed that the resultant inductive effect is equivalent to several hundred nH, which lowered the resonant frequency from the simulated 6 MHz in Section II-A to the measured 4.125 MHz. To verify that this inductive loading was responsible for the drop in the frequency value,

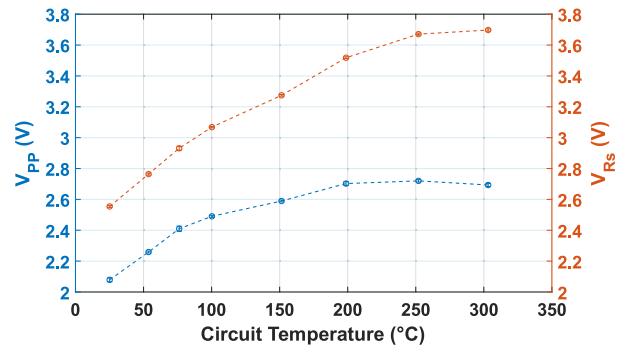


FIGURE 14. Oscillator circuit output voltage characteristics vs. temperature for oscillator circuit powered by TEGs and booster circuit. Left axis (blue curve) shows the oscillator peak-peak voltage (V_{PP}) for different circuit temperatures. Right axis (red curve) shows the dc biasing voltage across the source resistor R_S , for different oscillator operational temperatures. Note: the dashed lines connect the mean of each set of data points at each temperature. Data points for V_{PP} and V_{RS} represent the mean value of 12 measurements and the error bars represent ± 1 standard deviation.

a consumer grade 1 μ F surface mount bypass capacitor was connected between the V_{DD} point and ground at the output of the Inconel cable in the circuit shown in Fig. 5. The resonance frequency shifted upwards to 5.5 MHz, a difference from the 6 MHz design frequency that is within the tolerance limits of the inductor, capacitors, and MOSFET used in the experiment. However, this capacitor was needed to be removed for HT testing, as it was not rated for operation beyond 150 °C. Therefore, a sufficiently large value supply bypass capacitor capable of operation at HT could not only contribute to diminish the voltage ripple at the output of the TEG (Fig. 12 discussed above), but also remove the loading effect of the HT coaxial cable connecting the booster to the circuit.

Fig. 14 plots both the peak-to-peak oscillator output voltage, V_{PP} , and V_{RS} , the dc offset of the oscillator output voltage at the transistor source node, for measurements taken from room temperature to 300 °C. The increase in V_{PP} as the temperature increases is consistent with the MOSFET increase in drain current I_D with temperature shown in Fig. 9. The increase in V_{RS} with temperature up to 200 °C reveals an increase in average current and power consumption up to that temperature, followed by a stabilization between 200 °C and 300 °C, due to the stabilizing effect of the negative feedback provided by the source resistor R_S (Fig. 1).

The results reported in this section demonstrate the successful operation of the entire standalone system, powered by passively cooled TEGs, over a range of temperatures spanning from room temperature to 300 °C.

E. MEASUREMENT OF WIRELESS SIGNAL TRANSMITTED FROM OSCILLATOR AT HT

Fig. 15 plots the power spectrum of the wireless signal detected by the receiver antenna and the spectrum analyzer shown in Fig. 8. For this measurement, the oscillator circuit was operating at 300 °C, the TEGs heated plate was operated at 170 °C, and the receiving antenna was placed at

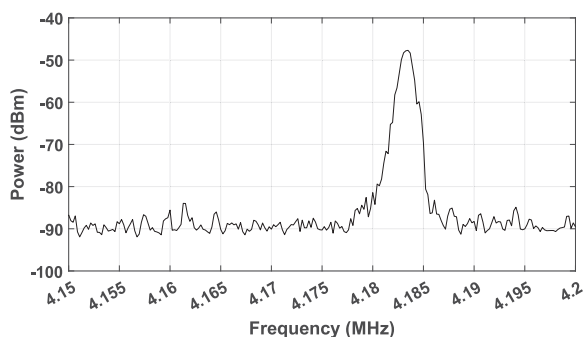


FIGURE 15. Frequency spectrum of the wireless signal received at 11 feet (3.4 m) from the full TEG/booster/oscillator system operating at 300 °C, powered by TEGs heated to 170 °C. Wireless signal was measured using the receiver antenna connected to a spectrum analyzer.

11 feet (3.4 m) from the oscillator circuit. The wirelessly detected free-running oscillator signal with a magnitude of -47 dBm at approximately 4.184 MHz can be clearly seen in Fig. 15.

These data confirm the successful transmission of a wireless signal from inside the HT environment to an external receiver, using a self-powered integrated oscillator and TEG energy-scavenging unit for standalone operation.

V. CONCLUSION

This article has successfully demonstrated a wireless, HT oscillator circuit, powered by energy-scavenging TEGs that are passively cooled. The oscillator circuit has been shown to operate from room temperature up to 300 °C, with a wireless signal range of at least 11 feet (3.4 m). This article demonstrates key components of a standalone, HT self-powered sensor platform that is capable of supplying both thermally scavenged power and wireless signal transmission for operating HT integrated sensors and other electronics. Future article should focus on replacing the room-temperature booster circuit with a robust HT alternative. Potential approaches to reach operation above 300 °C include the development of an HT booster circuit, or the implementation of a sufficiently large HT bypass capacitor, or yet the use of a HT charging battery. Long-term operational stability of the MOSFET and the other oscillator circuit components at HT should also be studied.

DISCLAIMER

This report was prepared as an account of work sponsored by an agency of the United States Government. Neither the United States Government nor any agency thereof, nor any of their employees, makes any warranty, express or implied, or assumes any legal liability or responsibility for the accuracy, completeness, or usefulness of any information, apparatus, product, or process disclosed, or represents that its use would not infringe privately owned rights. Reference herein to any specific commercial product, process, or service by trade name, trademark, manufacturer, or otherwise does not necessarily constitute or imply its endorsement, recommendation,

or favoring by the United States Government or any agency thereof. The views and opinions of authors expressed herein do not necessarily state or reflect those of the United States Government or any agency thereof.

ACKNOWLEDGMENT

The authors would like to acknowledge the contributions of Mr. Jude Zanoni who helped to design and simulate the custom planar-spiral inductors used in this article; and Mr. Conlan Taylor for helping with the fabrication of the HT circuit boards that were used to implement the oscillator circuits. The authors would also like to thank Mr. Shannon Scott for his help with HT MOSFET testing and characterization using the Keithley Semiconductor Characterization System, and Dr. Robert Lad for helpful discussions regarding testing and evaluation of the fabricated HT circuit boards.

REFERENCES

- [1] P. M. Castro, I. E. Grossmann, P. Veldhuizen, and D. Esplin, "Optimal maintenance scheduling of a gas engine power plant using generalized disjunctive programming," *AIChE J.*, vol. 60, no. 6, pp. 2083–2097, Feb. 2014, doi: [10.1002/aic.14412](https://doi.org/10.1002/aic.14412).
- [2] A. A. Nayeem, R. Venkatesan, and F. Khan, "Monitoring of down-hole parameters for early kick detection," *J. Loss Prevention Process Ind.*, vol. 40, pp. 43–54, Mar. 2016, doi: [10.1016/j.jlp.2015.11.025](https://doi.org/10.1016/j.jlp.2015.11.025).
- [3] C. Wu, S. Yang, G. Wen, and C. Fan, "A self-powered vibration sensor for downhole drilling tools based on hybrid electromagnetic-triboelectric nanogenerator," *Rev. Sci. Instrum.*, vol. 92, no. 5, May 2021, Art. no. 055003, doi: [10.1063/5.0040657](https://doi.org/10.1063/5.0040657).
- [4] A. Willersrud, M. Blanke, L. Imsland, and A. Pavlov, "Fault diagnosis of downhole drilling incidents using adaptive observers and statistical change detection," *J. Process Control*, vol. 30, pp. 90–103, Jun. 2015, doi: [10.1016/j.jprocont.2014.12.010](https://doi.org/10.1016/j.jprocont.2014.12.010).
- [5] T. H. Nguyen, P. T. Nguyen, and F. Garnier, "Evaluation of the relationship between the aerothermodynamic process and operational parameters in the high-pressure turbine of an aircraft engine," *Aerosp. Sci. Technol.*, vol. 86, pp. 93–105, Mar. 2019, doi: [10.1016/j.ast.2019.01.011](https://doi.org/10.1016/j.ast.2019.01.011).
- [6] J. Zhai, B. Sun, and Y. Zhou, "Failure analysis on 304 stainless steel tube of semi water gas preheater in coal chemical plant," *Eng. Failure Anal.*, vol. 125, Jul. 2021, Art. no. 105443, doi: [10.1016/j.engfailanal.2021.105443](https://doi.org/10.1016/j.engfailanal.2021.105443).
- [7] M. Pereira da Cunha, "Wireless sensing in hostile environments," in *Proc. IEEE Int. Ultrasonics Symp.*, 2013, pp. 1337–1346, doi: [10.1109/ULTSYM.2013.0342](https://doi.org/10.1109/ULTSYM.2013.0342).
- [8] P. G. Neudeck et al., "Year-long 500 °C operational demonstration of up-scaled 4H-SiC JFET integrated circuits," *J. Microelectron. Electron. Packag.*, vol. 15, pp. 163–170, Oct. 2018, doi: [10.4071/imaps.729648](https://doi.org/10.4071/imaps.729648).
- [9] P. G. Neudeck, D. J. Spry, L. Chen, N. F. Prokop, and M. J. Krasowski, "Demonstration of 4H-SiC digital integrated circuits above 800 °C," *IEEE Electron Device Lett.*, vol. 38, no. 8, pp. 1082–1085, Aug. 2017, doi: [10.1109/led.2017.2719280](https://doi.org/10.1109/led.2017.2719280).
- [10] A. Padhy, S. Joshi, S. Bitragunta, V. Chamola, and B. Sikdar, "A survey of energy and spectrum harvesting technologies and protocols for Next generation Wireless networks," *IEEE Access*, vol. 9, pp. 1737–1769, 2021, doi: [10.1109/access.2020.3046770](https://doi.org/10.1109/access.2020.3046770).
- [11] P. Sundriyal and S. Bhattacharya, "Energy harvesting techniques for powering wireless sensor networks in aircraft applications: A review," in *Sensors for Automotive and Aerospace Applications*. Singapore: Springer, 2018, pp. 55–76.
- [12] R. Wang, W. H. Ko, and D. J. Young, "Silicon-carbide MESFET-based 400C MEMS sensing and data telemetry," *IEEE Sensors J.*, vol. 5, no. 6, pp. 1389–1394, Dec. 2005, doi: [10.1109/JSEN.2005.858927](https://doi.org/10.1109/JSEN.2005.858927).
- [13] M. C. Scardelletti et al., "Wireless capacitive pressure sensor operating up to 400 °C from 0 to 100 PSI utilizing power scavenging," in *Proc. IEEE Topical Conf. Wireless Sensors Sensor Netw.*, 2014, pp. 34–36, doi: [10.1109/WISNet.2014.6825503](https://doi.org/10.1109/WISNet.2014.6825503).

- [14] J. L. Jordan, G. E. Ponchak, D. J. Spry, and P. G. Neudeck, "A high frequency (HF) inductive power transfer circuit for high temperature applications using SiC Schottky diodes," in *Proc. IEEE Topical Conf. Wireless Sensors Sensor Netw.*, 2018, pp. 23–26, doi: [10.1109/WISNET.2018.8311554](https://doi.org/10.1109/WISNET.2018.8311554).
- [15] A. Rahman, A. M. Francis, S. Ahmed, S. K. Akula, J. Holmes, and A. Mantooth, "High-temperature voltage and current references in silicon carbide CMOS," *IEEE Trans. Electron Devices*, vol. 63, no. 6, pp. 2455–2461, Jun. 2016, doi: [10.1109/ted.2016.2550580](https://doi.org/10.1109/ted.2016.2550580).
- [16] D. G. Senesky, B. Jamshidi, K. B. Cheng, and A. P. Pisano, "Harsh environment silicon carbide sensors for health and performance monitoring of aerospace systems: A review," *IEEE Sensors J.*, vol. 9, no. 11, pp. 1472–1478, Nov. 2009, doi: [10.1109/jsen.2009.2026996](https://doi.org/10.1109/jsen.2009.2026996).
- [17] Y. I. Shtern, D. G. Gromov, M. Y. Shtern, A. A. Sherchenkov, and M. S. Rogachev, "Multisectional thermoelement for generators working at the temperatures up to 1200 K," in *Proc. IEEE Conf. Russian Young Res. Elect. Electron. Eng.*, 2017, pp. 1201–1204, doi: [10.1109/EICor-Rus.2017.7910776](https://doi.org/10.1109/EICor-Rus.2017.7910776).
- [18] T. C. Holgate, R. Bennett, T. Hammel, T. Caillat, S. Keyser, and B. Sievers, "Increasing the efficiency of the multi-mission radioisotope thermoelectric generator," *J. Electron. Mater.*, vol. 44, no. 6, pp. 1814–1821, 2015, doi: [10.1007/s11664-014-3564-9](https://doi.org/10.1007/s11664-014-3564-9).
- [19] Y. Xie, S. Wu, and C. Yang, "Generation of electricity from deep-sea hydrothermal vents with a thermoelectric converter," *Appl. Energy*, vol. 164, pp. 620–627, Feb. 2016, doi: [10.1016/j.apenergy.2015.12.036](https://doi.org/10.1016/j.apenergy.2015.12.036).
- [20] T. Y. Kim, A. A. Negash, and G. Cho, "Waste heat recovery of a diesel engine using a thermoelectric generator equipped with customized thermoelectric modules," *Energy Convers. Manage.*, vol. 124, pp. 280–286, Sep. 2016, doi: [10.1016/j.enconman.2016.07.013](https://doi.org/10.1016/j.enconman.2016.07.013).
- [21] D. Champier, "Thermoelectric generators: A review of applications," *Energy Convers. Manage.*, vol. 140, pp. 167–181, May 2017, doi: [10.1016/j.enconman.2017.02.070](https://doi.org/10.1016/j.enconman.2017.02.070).
- [22] K. Sun et al., "Self-powered through-wall communication for dry cask storage monitoring," *Ann. Nucl. Energy*, vol. 177, Nov. 2022, Art. no. 109306.
- [23] Q. Lin, Y.-C. Chen, F. Chen, T. DeGanyar, and H. Yin, "Design and experiments of a thermoelectric-powered wireless sensor network platform for smart building envelope," *Appl. Energy*, vol. 305, Jan. 2022, Art. no. 117791, doi: [10.1016/j.apenergy.2021.117791](https://doi.org/10.1016/j.apenergy.2021.117791).
- [24] T. A. Carstens et al., "Thermoelectric powered wireless sensors for dry-cask storage," *IEEE Trans. Nucl. Sci.*, vol. 60, no. 2, pp. 1072–1079, Apr. 2013, doi: [10.1109/TNS.2012.2222664](https://doi.org/10.1109/TNS.2012.2222664).
- [25] J. Chen et al., "A thermoelectric energy harvesting system for powering wireless sensors in nuclear power plants," *IEEE Trans. Nucl. Sci.*, vol. 63, no. 5, pp. 2738–2746, Oct. 2016, doi: [10.1109/TNS.2016.2606090](https://doi.org/10.1109/TNS.2016.2606090).
- [26] A. S. Sedra and K. C. Smith, "LC and crystal oscillators," in *Microelectronic Circuits*. New York, NY, USA: Oxford Univ. Press, 2010, pp. 1349–1352.
- [27] G. Gonzalez, "Oscillation conditions," in *Foundations of Oscillator Circuit Design*. Boston, MA, USA: Artech House, 2007, pp. 1–5.
- [28] A. S. Sedra and K. C. Smith, "MOS field-effect transistors (MOS-FETs)," in *Microelectronic Circuits*, vol. 238. New York, NY, USA: Oxford Univ. Press, 2010, pp. 243.
- [29] "CPM3-1200-0075A Rev. 2, 03-2020," 2020. Accessed: Jun. 29, 2023. [Online]. Available: https://assets.wolfspeed.com/uploads/2020/12/cpm3_1200_0075a_external_version.pdf
- [30] C. Wang et al., "Contributed review: Instruments for measuring Seebeck coefficient of thin film thermoelectric materials: A mini-review," *Rev. Sci. Instrum.*, vol. 89, no. 10, Oct. 2018, Art. no. 101501, doi: [10.1063/1.5038406](https://doi.org/10.1063/1.5038406).
- [31] S. C. Moulzolf, R. Behanan, T. Pollard, R. J. Lad, and M. Pereira da Cunha, "Capacitively coupled IDT for high temperature SAW devices," in *Proc. IEEE Int. Ultrasonics Symp.*, 2013, pp. 255–258, doi: [10.1109/ULTSYM.2013.0066](https://doi.org/10.1109/ULTSYM.2013.0066).
- [32] J. M. Lopera, H. del Arco Rodríguez, J. M. Pérez Pereira, A. R. de Castro, and J. L. Rendueles Vigil, "Practical issues in the design of wireless sensors supplied by energy harvesting thermoelectric generators," *IEEE Trans. Ind. Appl.*, vol. 55, no. 1, pp. 996–1005, Jan./Feb. 2019, doi: [10.1109/TIA.2018.2867810](https://doi.org/10.1109/TIA.2018.2867810).



SHANE WINTERS (Student Member, IEEE) received the B.S. degree in electrical and computer engineering in 2006 and the M.S. degree in electrical engineering in 2011 from the University of Maine, Orono, ME, USA, where he is currently working toward the Ph.D. degree in electrical engineering with the Department of Electrical and Computer Engineering.

From 2012 to 2020, he worked with the MathWorks (Natick, MA, USA), with work primarily focused on software testing. His research interests

include high-temperature/hostile environment sensing, surface acoustic wave resonators, and dynamic strain sensing. His research interests also include bulk acoustic wave sensors for sensing mechanical and electrical properties in liquids.



NIKUNG THAPA received the bachelor's degree in electronics and communication engineering from the Tribhuvan University, Pokhara-lamachaur, Nepal, in 2017. He is currently working toward the M.S. degree in electrical engineering with the Department of Electrical and Computer Engineering, the University of Maine, Orono, ME, USA.

He is currently working as a Teaching Assistant with the ECE Department and as a Research Assistant with the Frontiers Institute of Research in Sensor Technologies Lab, University of Maine. He worked as an Electronics Engineer with the Avian Engineering Services Pvt. Ltd (2017–2020) and also as a part time Lecturer with the Lumbini Engineering College (2020–2021), Bhalwari, Nepal. His research interests include silicon carbide based high-temperature oscillator circuits.



LUKE D. DOUCETTE received the M.S. degree in physics from the University of Maine, Orono, ME, USA, in 2002.

He is currently a Senior Research Scientist with the University of Maine. His research interests include MBE thin film synthesis and characterization, optical sensors, semiconductor materials and devices, and high-temperature electronic systems and packaging.

Mr. Doucette was also a founding member and Senior Research Scientist with the OSS Inc., where he developed new products for the low-level detection of pollutants for environmental and industrial monitoring applications. As a result of his work in this area, he was the recipient of the 2013 Tibbetts Award for Excellence in Commercialization issued by the Small Business Administration.



JONATHAN KINCAID (Member, IEEE) received the B.Sc. degree in electrical engineering, University of Maine, Orono, ME, USA, in 2020.

He was previously an Employee of the Frontiers Institute for Research in Sensor Technologies (2020–2021) and Environetix Technologies Corp. (2019–2020). His research interests include high-temperature wireless sensing and energy scavenging for wireless applications.

Mr. Kincaid has been a member of HKN.



QINGSONG CUI received the Ph.D Degree in measurement technology and instruments from Beihang University, Beihang, China, in 2013.

He is currently an Assistant Professor of Engineering with the Valdosta State University, Valdosta, GA, USA. His research interests include fiber optics, nanomaterials, RF engineering, and wireless sensors.



NURI W. EMANETOGLU (Member, IEEE) received the B.S. degree in electronics and communications engineering from the Istanbul Technical University, Istanbul, Turkey, in 1995, and the M.S. and Ph.D. degrees in electrical and computer engineering from the Rutgers University, New Brunswick, NJ, USA, in 1998 and 2003, respectively.

He is currently an Associate Professor of Electrical and Computer Engineering with the University of Maine, Orono, ME, USA. He was a Postdoctoral

Research Associate with the Rutgers (2003–2004), and an ORAU Postdoctoral Research Fellow with the U.S. Army Research Laboratory (2005–2006) prior to UMaine. His research interests include modeling, fabrication, and characterization of solid-state devices based on acoustic, optical, and electronic interactions and their applications to communications systems and sensor technologies. He has authored/coauthored 33 journal articles, 31 conference proceedings, 1 book, and 1 book chapter, and he has 8 patents.

Dr. Emanetoglu is a member of the ASEE.



MAURICIO PEREIRA DA CUNHA (Senior Member, IEEE) received the bachelor's and master's degrees (Hons.) in electrical engineering from the Escola Politécnica, Universidade de São Paulo, São Paulo, Brazil, in 1985 and 1989, respectively, and the Ph.D. degree (Hons.) in electrical engineering from the McGill University, Montreal, PQ, Canada, in 1994.

He is currently a Roger Clapp Castle and Virginia Averill Castle Professor of Electrical and Computer Engineering with the University of

Maine, Orono, ME, USA, and a CEO of the Environetix Technologies Corp. During his sabbatical (1999/2000) at the University of Central Florida, he worked with Consortium for Applied Acoustoelectronic Technology, Orlando, FL, USA, and in cooperation with the Piezotechnology Inc. He has also worked with the SAWTEK Inc. (now Qorvo), Orlando, FL, USA; McGill University, Montreal, PQ, Canada; Laboratório de Microeletrônica, Escola Politécnica, Universidade de São Paulo; and with the Microwave Devices R&D Group at NEC (Nippon Electric Co.), Brazil. His research interests include harsh environment sensors, wireless, gas and biomedical sensors, antennas, microwave acoustic modeling, devices, and propagation (>270 publications).

Dr. Pereira da Cunha is a member of the Sigma Xi, and the Brazilian Microwave Society.